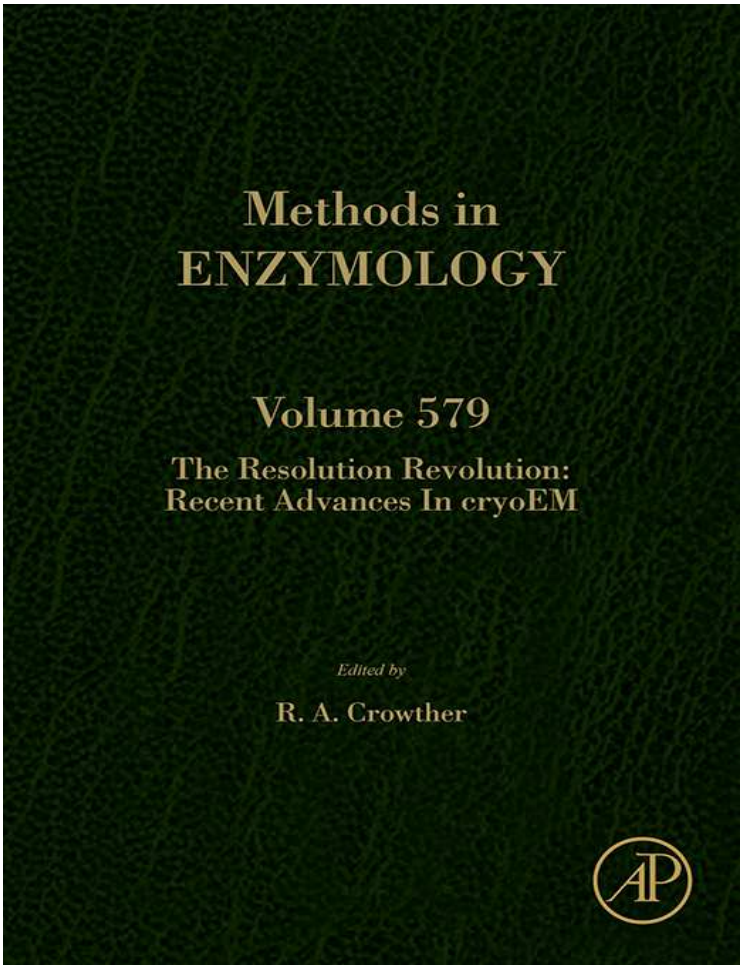

From J.A. Rodriguez and T. Gonen, High-Resolution Macromolecular Structure Determination by MicroED, a cryo-EM Method. In: R.A. Crowther, editor, *Methods in Enzymology, Vol. 579*, Burlington: Academic Press, 2016, pp. 369-392.
ISBN: 978-0-12-805382-9

CHAPTER FOURTEEN

High-Resolution Macromolecular Structure Determination by MicroED, a cryo-EM Method

J.A. Rodriguez*, T. Gonen†,1
*UCLA-DOE Institute, University of California, Los Angeles CA, United States
†Janelia Research Campus, Howard Hughes Medical Institute, Ashburn VA, United States
1Corresponding author: e-mail address: gonent@janelia.hhmi.org

Contents

1. Introduction 370
2. Background 371
   2.1 Origins of Electron Diffraction 371
   2.2 Transmission Electron Microscopy and Diffraction 371
   2.3 Electron Diffraction of Protein Assemblies 372
   2.4 Electron Diffraction of 3D Protein Crystals: MicroED 373
3. Sample Preparation 378
   3.1 Approaches to Growth and Screening of Crystals for MicroED 378
   3.2 Cryo-Preservation of Nanocrystals for MicroED 379
4. Instrumentation and Data Collection 380
   4.1 Electron Source Specifications 380
   4.2 Electron Optics Specifications 380
   4.3 Energy Filtering 382
   4.4 Low-Dose Data Collection 383
   4.5 Detector Specifications 384
5. Processing of MicroED Data 384
   5.1 Conversion and Processing of Diffraction Images 384
   5.2 Structure Determination and Refinement 387
6. Summary and Outlook 388
Acknowledgments 388
References 389

Abstract

Microelectron diffraction (MicroED) is a new cryo-electron microscopy (cryo-EM) method capable of determining macromolecular structures at atomic resolution from vanishingly small 3D crystals. MicroED promises to solve atomic resolution structures from even the tiniest of crystals, less than a few hundred nanometers thick. MicroED complements frontier advances in crystallography and represents part of the rebirth of cryo-EM that is making macromolecular structure determination more accessible

Methods in Enzymology, Volume 579
ISSN 0076-6879
http://dx.doi.org/10.1016/bs.mie.2016.04.017

for all. Here we review the concept and practice of MicroED, for both the electron microscopist and crystallographer. Where other reviews have addressed specific details of the technique (Hattne et al., 2015; Shi et al., 2016; Shi, Nannenga, Iadanza, & Gonen, 2013), we aim to provide context and highlight important features that should be considered when performing a MicroED experiment.

1. INTRODUCTION

Over the past century, X-ray crystallography has revealed the structures of thousands of macromolecules. Today, the frontier of structural biology is rapidly being expanded by cryo-electron microscopy (cryo-EM) thanks to a new generation of electron microscopes and detectors, and the emergence of new techniques (Cheng, Grigorieff, Penczek, & Walz, 2015; Shi, Nannenga, Iadanza, & Gonen, 2013). Four cryo-EM methods benefit from these improvements: tomography, single particle, 2D electron crystallography, and microelectron diffraction (MicroED). MicroED is a cryo-EM method that determines atomic resolution structures from three-dimensional protein crystals only hundreds of nanometers in thickness and in doing so promises to provide a new approach to structure determination of macromolecular structures (Shi et al., 2013). MicroED leverages infrastructure created by X-ray crystallography for structure determination while exploiting the strong interaction between electrons and the crystal (Henderson, 1995; Nannenga & Gonen, 2014). This strong interaction arises from the intrinsic nature of electrons as charged particles. Electrons have a higher scattering cross-section and are sensitive to charge. Magnetic lenses can be used to focus electrons and produce high-resolution images or diffraction and, on a practical note, electron microscopes are more accessible and less expensive than high-flux X-ray sources. New electron sources can even generate ultrafast pulses that probe matter at femtosecond timescales (Weathersby et al., 2015). Empowered by these new methods, electron microscopists can now determine the structures of protein molecules at high resolutions from images (Cheng et al., 2015) or diffraction (Rodriguez et al., 2015), and produce atomic resolution structures from crystals one protein layer thick (Gonen et al., 2005). In what follows we present a brief overview of electron diffraction and review the tools and techniques used by MicroED.

2. BACKGROUND

2.1 Origins of Electron Diffraction

The wave nature of the electron was first confirmed by diffraction of electrons from a crystal of nickel in 1927. The demonstration by Davisson and Germer using low-energy electrons (Davisson & Germer, 1927a, 1927b) linked their scattering properties to the de Broglie wavelength. The experiment was echoed shortly thereafter by Thomson and Reid who used higher energy electrons to observe diffraction from a thin celluloid film (Thomson & Reid, 1927). These first experiments highlight unique properties of electrons compared to X-rays: electrons benefit from intrinsically higher scattering and are easier to manipulate than X-rays, but are also limited in ways that X-rays are not. The inelastic mean free path of electrons is much shorter than for X-rays (Bethe, Rose, & Smith, 1938). Accordingly, samples analyzed by electrons must be smaller than those analyzed by X-rays. This limits electron diffraction (particularly using low-energy electrons) to the analysis of surface atomic layers in a thick crystal (Held, 2012). Higher energy electrons can penetrate thin inorganic nanoparticles and submicron thick organic structures. Using high-energy electron diffraction, structures can be obtained from micron-sized organic crystals that are thin and radiation resistant (Dorset & Hauptman, 1976). However, structure determination by electron diffraction from macromolecular crystals that are sensitive to radiation has required the development of specialized methods in cryo-EM (Shi et al., 2013).

2.2 Transmission Electron Microscopy and Diffraction

The first transmission electron micrograph was captured from magnified images of mesh grids in 1931 through the use of magnetic lenses. For their continuous improvement of electron microscope designs and progress toward the modern microscope, Ernst Ruska, Gerd Binnig, and Heinrich Rohrer would go on to win the Nobel prize in physics in 1986 (Robinson, 1986). Technical improvements and the invention of new devices for electron manipulation during the age of film detectors would build toward the success of modern microscopes. New lens configurations (Cowley, 1969), spatial filters (Danev & Nagayama, 2001), energy discriminators (Henkelman & Ottensmeyer, 1974), and aberration correctors

(Haider et al., 1998) would improve image quality and reduce artifacts (Batson, Dellby, & Krivanek, 2002). Automation and digitization have increased microscope stability and reproducibility of image acquisition (Koster, Chen, Sedat, & Agard, 1992). For biological specimens, cryogenic techniques (Adrian, Dubochet, Lepault, & McDowall, 1984; Christensen, 1971; Cowley, 1964; Taylor & Glaeser, 1976), detector improvements (Cheng et al., 2015; Ruskin, Yu, & Grigorieff, 2013), and new data collection and analysis methods (Shi et al., 2013) have driven the modern revolution in cryo-EM.

The transmission electron microscope (TEM) has made high-resolution imaging and diffraction accessible, but concerns about absorption and multiple-scattering phenomena have curbed the widespread determination of atomic resolution structures obtained using electron diffraction measurements. Electron diffraction even from thin inorganic crystals is influenced by nonkinematical scattering that perturbs its intensities, limiting determination of their structure by crystallographic means (Stern & Taub, 1970). Despite these challenges, in 1976 direct phasing from electron diffraction data was accomplished on an organic compound (Dorset & Hauptman, 1976), demonstrating the potential of electron crystallography at atomic resolution. Meanwhile, in the 1960s, Aaron Klug and colleagues pioneered the use of quantitative electron microscopy for structural studies of biomolecules at the MRC Laboratory of Molecular Biology in Cambridge (Crowther, DeRosier, & Klug, 1970; DeRosier & Klug, 1968). Their efforts forged the path to computerized image processing of TEM images and the 3D reconstruction of macromolecules by electron microscopy. These milestones set the stage for the use of electron diffraction in high-resolution structure determination from ordered protein assemblies, an achievement realized by Henderson and Unwin with their structure of bacteriorhodopsin (Henderson & Unwin, 1975). This was an effort nearly 20 years in the making that culminated in an atomic model of the protein in the early 1990s from 2D crystals (Henderson et al., 1990). Since these initial demonstrations, 2D electron crystallography has produced a handful of high-resolution structures of membrane proteins.

2.3 Electron Diffraction of Protein Assemblies

The study of ordered protein assemblies by electron microscopy dates back to the structure of T4 bacteriophage tails (DeRosier & Klug, 1968). Reconstruction of these assemblies relied on the helical nature of the tails. Similarly,

2D arrays of simple molecules with regular packing could be studied. Since an electron beam can diffract from even a single layer of molecules, thin crystals became an ideal target for electron diffraction. Among the first of these assemblies to be investigated was of a light-driven proton pump in *Halobacterium salinarum*, a transmembrane protein named bacteriorhodopsin or bR for short. This channel constitutes the protein fraction of a 2D crystal known as purple membrane, which exists naturally as part of the membrane of *H. salinarum*. By the mid-1970s Henderson and Unwin had achieved a 7 Å model of bR from a combination of electron diffraction patterns and electron micrographs (Henderson & Unwin, 1975). Over the next decades, their structure would improve to reach atomic resolution (Henderson et al., 1990). While the photoreaction complex would be the first membrane protein structure uncovered by crystallography using X-ray methods (Deisenhofer, Epp, Miki, Huber, & Michel, 1985), the structure of bR would open the door to 2D electron crystallography of a number of other membrane proteins. Structures of the light-harvesting chlorophyll a/b-protein complex (Kühlbrandt, Wang, & Fujiyoshi, 1994), of PhoE porin (Jap, Downing, & Walian, 1990), of aquaporin (Gonen, Sliz, Kistler, Cheng, & Walz, 2004; Hiroaki et al., 2006; Walz et al., 1997), and several others have been deciphered by 2D electron crystallography. Of these, the structure of the lens-specific water pore, aquaporin-0, shows the highest resolution at 1.9 Å (Gonen et al., 2005). The atomic model built for this structure includes coordinates for surrounding lipids and shows details of channel–lipid interactions. It is important to note that for a 2D crystal the phases of the diffraction spots can be recovered from Fourier transforms of images of the crystal, so a 3D map can be directly calculated.

2.4 Electron Diffraction of 3D Protein Crystals: MicroED

The success of 2D electron crystallography is limited by the need to produce well-ordered 2D crystals from proteins (Walz & Grigorieff, 1998). While collection of data is well established (Gonen, 2013), growing 2D crystals remains a challenge. Meanwhile cryo-EM has expanded to include a new method developed by Tamir Gonen and colleagues that marries approaches from electron and X-ray crystallography (Shi et al., 2013). The method, named MicroED, is short for 3D microelectron diffraction (Nannenga & Gonen, 2014). In MicroED, diffraction patterns are collected from submicron thick 3D crystals using a focused low-dose electron beam under cryogenic temperatures. Sampling a crystal at different orientations reveals its

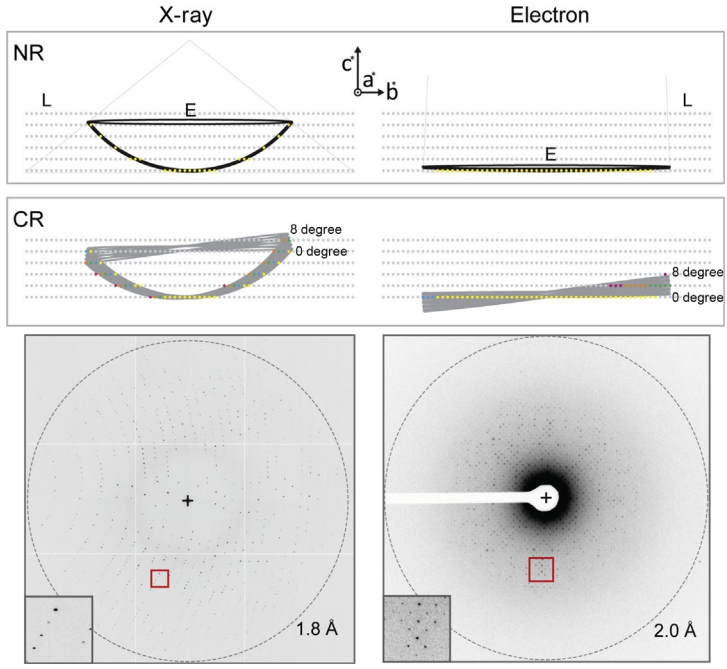

Fig. 1 Comparison between X-ray and electron crystallography. *Left* and *right* panels show schematic representations of two experimental geometries, X-ray (*left*) and electron (*right*) diffraction; distances and images are not to scale. The Ewald sphere (*E*), the *black shell outline* in both, displays significant curvature in X-ray diffraction; its curvature is hardly visible in the case of electron diffraction. The upper panel demonstrates a case where the crystal is kept fixed (*NR*, no rotation) and reflections are measured (*yellow*, *light gray* in the print version) as they intersect the Ewald sphere. The reciprocal lattice (*L*) is shown in light gray. Reciprocal lattice vectors are represented by a*, b*, and c*. The *middle panel* demonstrates the case where the crystal undergoes a uniform unidirectional rotation of 8 degree (*CR*, continuous rotation). As before, when reflections intersect the Ewald sphere they appear colored, first *yellow* (*light gray* in the print version), *blue* (*gray* in the print version), *green* (*gray* in the print version), *orange* (*light gray* in the print version), and *magenta* (*dark gray* in the print version). The *bottom panel* shows representative diffraction micrographs collected by X-ray and electron diffraction from 3D protein crystals. Insets show magnified areas of interest; the *circles denote resolution*.

reciprocal lattice and allows indexing of its structure factors (Fig. 1). The appeal of MicroED comes in part from its requirement for a simple reconfiguration of readily accessible, commercially available electron microscopy equipment (Table 1 and Fig. 2). MicroED allows macromolecular structure determination from submicron thick protein crystals whose structures might otherwise remain inaccessible. The method was first

Table 1 Technical Specifications of a MicroED Experiment

Property	Range
Energy	80–300 keV
Wavelength	0.0418–0.0197 Å
Camera length	200–6000 mm
Tilt range	±70 degree
Energy spread	0.2–3.0 eV

Ranges for energy, wavelength, camera length, tilt range, and energy spread are provided. Typical values for MicroED experiments using a standard TEM instrument are shown.

demonstrated on the well-known structure of lysozyme (Shi et al., 2013). Lysozyme crystals were preserved in a cryogenic state on a standard microscopy grid and diffracted to high resolution. Initially, diffraction patterns were indexed and integrated using custom software (Iadanza & Gonen, 2014). A set of low-dose diffraction patterns acquired at discrete angular increments resulted in a nearly complete data set that was phased by molecular replacement to produce a structure of lysozyme at 2.9 Å resolution (Shi et al., 2013). Shortly after that first demonstration, a continuous rotation approach to data collection (Fig. 1) produced better data with fewer artifacts from partial reflections and diminished multiple-scattering effects. The usefulness of the continuous rotation method was demonstrated on crystals of both lysozyme and catalase (Nannenga, Shi, Hattne, Reyes, & Gonen, 2014; Nannenga, Shi, Leslie, & Gonen, 2014) (Fig. 3). Meanwhile, a group led by Koji Yonekura in Japan worked to solve the structures of catalase and calcium ATPase from 3D crystals using a variation of the MicroED method (Yonekura, Kato, Ogasawara, Tomita, & Toyoshima, 2015). Added to this list is a recent high-resolution structure of proteinase K, determined by MicroED to 1.75 Å resolution (Hattne, Shi, de la Cruz, Reyes, & Gonen, 2016). In a collaborative effort, the groups of Tamir Gonen and David Eisenberg used MicroED to obtain the structure of two amyloid segments of 10 and 11 amino acids from the protein alpha-synuclein which forms pathological deposits in Parkinson's disease. The segments formed crystals a mere 200 by 200 by 1500 nanometers in size, only about an order of magnitude larger than an amyloid fibril. These are the first new structures determined by this method, and at 1.4 Å, the highest resolution structures determined by cryo-EM to date, and allowed determination of the positions of some protons (Rodriguez et al., 2015). In MicroED, as in X-ray

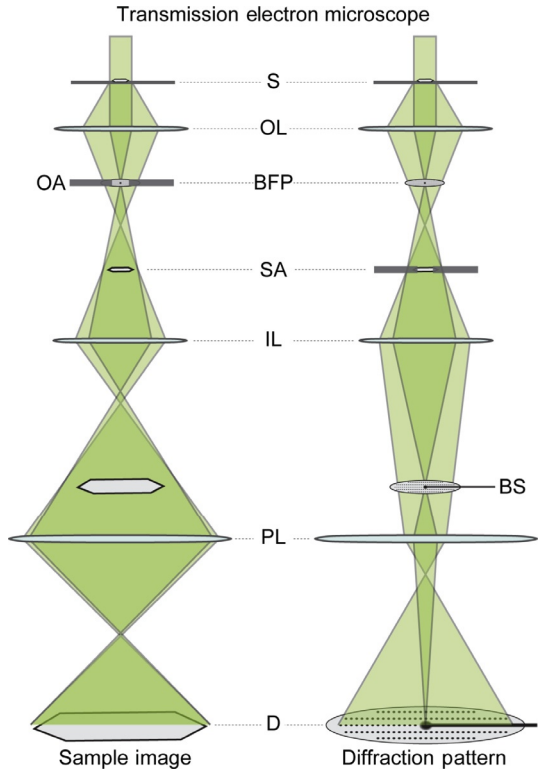

Fig. 2 Comparison of configurations of a transmission electron microscope for imaging and MicroED. A simplified ray diagram demonstrates the principle of each; components and distances are not to scale. A nearly parallel electron beam is shown impinging on a crystal sample (*S*), imaged by an objective lens (*OL*). The *left panel* shows the microscope configuration for obtaining an image of the sample in question; the *right* shows how to configure the microscope to obtain a diffraction pattern. The back focal plane (*BFP*) is shown in each. In imaging mode, a spatial filter, an objective aperture (*OA*) is placed at this plane to provide contrast. The selected area aperture (*SA*) is used to restrict diffraction to a specific region using an aperture as a spatial filter. An intermediate lens system follows (*IL*) which focuses on either the conjugate image plane (*left panel*) or back focal plane (*right panel*) of the objective lens to produce a magnified image or diffraction pattern. In diffraction mode, a beam stop (*BS*) can be placed within or after the projection lens system to obstruct measurement of the focused electron beam. A projection lens system (*PL*) renders the final image or diffraction pattern onto a detector (*D*).

diffraction, only the amplitudes of the diffracted beams are measured but the phases cannot be directly recovered from images in the way they are for 2D crystals, so structures must be solved by indirect means such as molecular replacement.

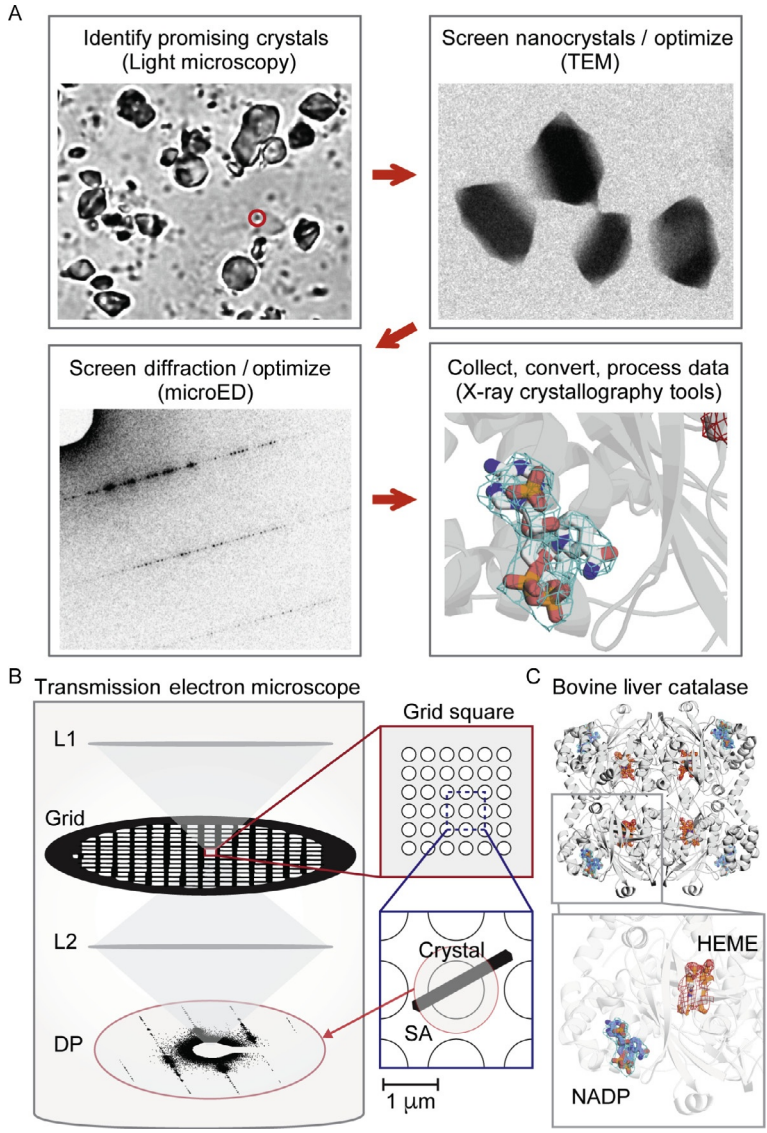

Fig. 3 Pipeline for structure determination by MicroED. (A) A simplified four step process is shown to summarize the process for macromolecular structure determination by MicroED. First, promising protein mixtures are screened by light microscopy for the presence of crystals then by electron microscopy for adequately sized crystals (*red circle* shows a 5 μm diameter). If crystals are present, they can immediately be screened for diffraction on the electron microscope. Diffraction can be optimized until high-resolution diffraction tilt series can be obtained for a given protein. These tilt series images can be converted to SMV format and processed using standard crystallography

(*Continued*)

3. SAMPLE PREPARATION

3.1 Approaches to Growth and Screening of Crystals for MicroED

A variety of techniques has been developed for growing protein crystals. At least two of these techniques are used routinely in MicroED experiments: the vapor diffusion technique and the batch approach to crystallization. In vapor diffusion protocols, a drop is prepared that contains both the macromolecule of interest and mother liquor solution, a cocktail of precipitants and ions. This drop is held in a closed environment in the presence of a reservoir solution. Over time, equilibration drives the protein concentration in the drop toward saturation and crystals form. In the batch experiment, a protein sits in mother liquor solution until crystals appear. Both of these preparations are screened visually for crystal formation using optical microscopes (Fig. 3). This screening process presents inherent limitations. If the crystals formed are smaller than the wavelength of visible light, resolving individual crystals by eye becomes difficult. This means submicron thick crystals ideal for MicroED might be missed, and since these crystals may not grow any larger, an opportunity to determine their structure is lost.

To overcome the bottleneck present in screening for tiny crystals, new high-throughput methods are being engineered. One possible solution is

Fig. 3—Cont'd software packages. Structure determination then follows the procedures established for X-ray crystallography to phase by molecular replacement. (B) Process by which diffraction is obtained from a 3D protein crystal using a transmission electron microscope. An electron beam is condensed (*L1*) and illuminates a protein crystal that sits vitrified on a holey carbon film (*inset, top*) within a meshed electron microscopy grid. A representation of the magnified *grid square* is shown to demonstrate the size of the illuminated area relative to the crystal, and the selected area (*inset, bottom*) from which a diffraction pattern (*DP*) is obtained at the back focal plane of a second lens or lens system (*L2*). Projection lenses (not shown, see Fig. 2) image this pattern onto an electronic detector, which digitally records this pattern. The grid containing the crystal can be rotated in a discrete or continuous fashion to produce patterns at various orientations from a single or multiple crystals. These patterns can be processed and phased to determine the structure of the molecule that formed the crystal. (C) In this example, the protein catalase was solved by MicroED to a resolution of 3.2 Å using the method of continuous rotation. A ribbon diagram of the protein is shown along with density for two ligands, a HEME group (*red mesh*, *orange sticks*), and an NADP molecule (*blue mesh*, *purple sticks*). These molecules were omitted from an initial model search during the molecular replacement protocol; their density was recovered during the refinement process (Nannenga, Shi, Hattne, et al., 2014). Renderings were generated using PDB ID 3J7B.

provided by second order nonlinear imaging of chiral crystals (SONICC), an optical technique that can be used to coarsely visualize crystals in solution. However, SONICC cannot universally detect protein crystals in solution, is limited by crystal size, is not useful for certain crystal symmetries, and thus cannot generally assess the diffracting quality of crystals (Haupert & Simpson, 2011). Instead, a more reliable approach to screening is by preparation of EM grids from a suspension of crystals and direct visualization and diffraction on an electron microscope (Fig. 3). Even the simple preparation of negative-stained crystal samples can provide fast insight into crystal quality. This makes evident the need for an electron microscope capable of routine and rapid screening of MicroED samples, to achieve high-throughput evaluation of potential crystals. Alternatively, X-ray-based screening can be conducted either by obtaining powder-like diffraction from a crystal slurry using large, weak X-ray probes or proof of single-crystal diffraction from single crystals using microfocus X-ray sources.

3.2 Cryo-Preservation of Nanocrystals for MicroED

Provided a crystal is found suitable for MicroED by the aforementioned screening methods, the crystal must then be cryo-preserved for subsequent diffraction. Cryo-sample preparation has been extensively reviewed for single particle and cellular studies (Glaeser, 2008; Grassucci, Taylor, & Frank, 2007; Iancu et al., 2007). Here we briefly introduce the concept of cryo-sample preparation of crystals, which draws strongly from preestablished methods. To summarize the procedure, we begin by placing a small volume of crystals suspended in mother liquor onto an EM grid. For ease of blotting, Quantifoil grids are used; these contain a thin carbon film (5–30 nm thick) with regularly sized and spaced holes, on a standard copper support mesh (typically 200–400 mesh). In these grids, a typical mesh square measures 40–80 μm on a side. The concentration of crystals can be optimized such that no more than a few microcrystals end up on any given grid square. Once a droplet with crystals is placed on a grid, freezing can proceed using manual instruments or robots that wick or blot excess mother liquor within a few seconds, then plunge the grid at high speed into a bath of liquid ethane or other cryogen (Dobro, Melanson, Jensen, & McDowall, 2010). Frozen grids can be transferred to liquid nitrogen for temporary or long-term storage and ultimately loaded onto a cryo-holder under liquid nitrogen. Although light microscopes can visualize grids under a liquid nitrogen environment to screen for quality of freezing (Lepper, Merkel, Sartori, Cyrklaff, & Frischknecht, 2010), their utility is limited for imaging crystals whose size is comparable to or smaller than the wavelength of light.

4. INSTRUMENTATION AND DATA COLLECTION

4.1 Electron Source Specifications

While electron diffraction can be performed on almost any electron microscope, high-resolution diffraction is most likely to be obtained using modern microscopes equipped with field emission electron guns (FEGs). The electron gun in a microscope ultimately dictates the quality of the beam used for diffraction. In field emission guns the ejection of electrons is induced by an electrostatic field from a narrow tip. Compared to filament-based sources, FEGs produce electron beams that are brighter, stable, and more coherent. Diffraction is subject to the effects of both temporal and spatial coherence; these have been extensively reviewed elsewhere (Morishita, Yamasaki, & Tanaka, 2013; Zuo et al., 2004). We present a brief summary of temporal and lateral coherence and their relevance to 3D protein crystals. Temporal coherence is dictated by the chromatic or energy spread of the electron beam. Both the energy of an electron beam and its intrinsic spread are determined by the configuration of its source. Modern field emission guns can operate at a range of energies, with stable configurations typically ranging from 80 to 300 keV. The energy spread for field emission sources is narrower than for thermal emitters (eg, filaments), and can be as low as a fraction of an eV, or less than 0.0005% for a 200 keV beam (Table 1). A simple test for overall coherence is diffraction from slits or a small aperture. Provided proper beam collimation is achieved, a sufficiently coherent electron beam can be obtained (Morishita et al., 2013).

4.2 Electron Optics Specifications

The design of lens configurations varies between electron microscopes, even for a given manufacturer. Rather than present a particular configuration, we assume a general design in which the primary beam is condensed by a two or three lens system onto a sample, then imaged by an objective lens and focused onto a detector by a projector lens system as summarized in Fig. 2. The condenser lens system includes one or more apertures that serve to collimate the incident beam and improve its coherence. Apertures are typically positioned at the back focal plane of a corresponding lens and spatially restrict electrons that cross that plane. The sample stage is sandwiched closely between a condenser and objective lens pair (Fig. 2). Following the objective lens are two apertures, one positioned at its back focal plane and a second at its conjugate image plane. The aperture at its back focal plane is

termed the objective aperture (Fig. 2). It acts as a spatial frequency filter in the Fourier domain, akin to a digital low-pass filter. The second aperture is termed the selected area aperture (Fig. 2). This aperture limits the area to be imaged by the projector lens system. When this area is limited, the projector lens system can produce a diffraction pattern from the selected area alone (Fig. 3). This mode is termed selected area electron diffraction. As an electron diffraction technique, MicroED is performed by measuring either a full diffraction image from a given field of view, or a selected area diffraction image from a limited field of view.

Several systematic errors can occur in the beam path of an electron microscope that degrade electron micrographs. These must be avoided in a diffraction experiment. No microscope is perfect, so deviations from an ideal microscope have been the subject of many studies and have inspired the creation of corrective optics for electron lenses (Batson et al., 2002; Haider et al., 1998). The most relevant to diffraction-based techniques, including MicroED are astigmatism in the diffraction lens (the first projection lens) and beam collimation. Because electron diffraction patterns are generated by the objective and projector lens systems in a microscope, imperfections in these lenses limits the ability to properly focus the diffracted reflections onto the detector and can substantially interfere with the measured intensities in diffraction micrographs. To evaluate these errors, a test sample can be measured; catalase crystals, evaporated gold, and graphene are common test samples. Given the well-known structure of these samples, the effect of astigmatisms, aberrations, and misalignments in the electron optics can be assessed. The specifications for all protein crystals whose structures have been determined by MicroED so far, and which have been used for test purposes are detailed in Table 2. The structures of four prion peptides have also been solved at atomic resolution (Table 2). The structures of these segments from the yeast prion protein Sup35 were determined using ab initio methods from data collected by MicroED (Sawaya et al., in preparation).

A focused electron beam is prevented from impinging directly onto the detector by a beam stop positioned after the objective lens. In principle a Faraday device can be used as a beam stop to measure the transmitted and focused electron beam (Grubb, 1971). Beam stops can also be designed to minimize the obstruction of low-resolution information. Ultimately the lowest resolution sampling achievable is dictated by the effective camera length of a particular diffraction setting. The camera length is determined by the projection lens system and governs the resolution range and sampling of the reciprocal lattice. For example, crystals with large unit cells produce closely spaced reflections. The camera length must be optimized so that closely spaced reflections

Table 2 Structures Determined by MicroED

Sample	PDB ID	EMDB ID	Resolution (Å)	Space Group	Cell Dimensions a, b, c (Å) | α, β, γ (degree)
Lysozyme	3J4G	EMD-2945	2.9	P 43 21 2	77, 77, 37 | 90, 90, 90
Lysozyme	3J6K	EMD-6313	2.5	P 43 21 2	76, 76, 37 | 90, 90, 90
Catalase	3J7B	EMD-6314	3.2	P 21 21 21	68, 172, 182 | 90, 90, 90
Catalase	3J7U	–	3.2	P 21 21 21	69, 174, 206 | 90, 90, 90
Ca-ATPase	3J7T	–	3.4	C 1 2 1	166, 64, 147 | 90, 98, 90
Proteinase K	519S	EMD-8077	1.8	P 43 21 2	67, 67, 102 | 90, 90, 90
NACore	4RIL	EMD-3028	1.4	C 1 2 1	70.8, 4.8, 16.8 | 90, 106, 90
PreNAC	4ZNN	EMD-3001	1.4	P 1 21 1	17.9, 4.7, 33 | 90, 94, 90
Zn-NNQQNY	5K2E	EMD-8196	1.0	P 21	21.5, 4.9, 23.9 | 90, 104, 90
Cd-NNQQNY	5K2F	EMD-8197	1.0	P 21	22.1, 4.9, 23.5 | 90, 104.3, 90
GNNQQNY1	5K2G	EMD-8198	1.1	P 21	22.9, 4.9, 24.2 | 90, 107.8, 90
GNNQQNY2	5K2H	EMD-8199	1.05	P 21 21 21	23.2, 4.9, 40.5 | 90, 90, 90

can be accurately sampled as individual spots on a diffraction image. Measurement of reflections less than 50 Å in resolution proves a challenge on most conventional microscopes, so MicroED is not suitable for low-resolution studies.

4.3 Energy Filtering

As the thickness of a specimen grows, the ratio of inelastically to elastically scattered electrons can become significant. To alleviate this effect, a number of tools have been developed that can filter out inelastically scattered electrons and reduce their impact on measured diffraction patterns. This is because inelastically scattered electrons emerge from a sample with an energy that differs from that of their elastically scattered counterparts and the primary beam (Henkelman & Ottensmeyer, 1974; Zanchi, Sevely, & Jouffrey, 1977). Several types of energy filters are currently manufactured; all spatially separate the scattered electrons based on their respective energy. Some energy filters are located in column, and make up part of the optical train, while others are postcolumn filters that are placed just upstream of and couple to the detector. The energy spread of the primary beam is determined

by the properties of its source, while electrons that lose energy during their interactions with a crystal will have energies that differ beyond that intrinsic spread. Nonkinematic scattering of electrons can be further reduced by operating a microscope at higher energies, but under these conditions other damage mechanisms become prominent (Thomas, 1970; Zanchi et al., 1977).

4.4 Low-Dose Data Collection

To obtain diffraction micrographs from a single crystal of biological material at multiple orientations without destroying the crystal, a strategy must be employed to limit the dose given to the sample during the experiment. In MicroED, loss of high-resolution information can occur with doses over $9e^{-}/Å^2$ (Shi et al., 2013) in still diffraction but in continuous rotation with doses as low as $5e^{-}/Å^2$ (Nannenga, Shi, Hattne, et al., 2014; Nannenga, Shi, Leslie, et al., 2014). A very low-dose data collection strategy must be employed to overcome this limitation. The most efficient of these strategies involves a crystal being dosed in a discrete series of micrographs collected at various angles. However, this series of "still" diffraction patterns measures only partial reflections and is therefore not the most accurate way to recover true reflection intensities (Fig. 1). To integrate over full reflections, a unidirectional rotation of the crystal can be performed during continuous exposure to the electron beam (Nannenga, Shi, Leslie, et al., 2014). In this mode, the detector can be operated with line-by-line readout, termed rolling shutter integration. While better sampling full reflections, this type of readout suffers from higher detector noise and allows the crystal to be continuously dosed during data collection. Alternatively, as has been demonstrated with dose-insensitive inorganic specimens, precession can be used to collect still diffraction images that suffer less from partiality (Oleynikov, Hovmöller, & Zou, 2007). In such a case, instead of rotating the sample, the beam is tilted (Table 1). This efficiently exposes the crystal only during meaningful data acquisition intervals. In this scheme, the detector readout time can be longer and therefore images with lower readout noise can be acquired.

The dose of electrons can be tuned on a microscope by condensing or spatially restricting the electron beam. One way to achieve this is by limiting the spot size of the beam on the specimen as a result of a strong crossover produced by the first condenser lens. Condenser apertures can further reduce the size of the illuminating beam. While commercial field emission guns can achieve electron currents of 10^8 $e^{-}/Å^2/s$, the flux experienced by a crystal in a MicroED experiment is typically limited to 0.01 $e^{-}/Å^2/s$ or lower (Shi et al., 2013).

Detailed protocols for setting up the microscope for MicroED, data collection and analysis have been published recently (Shi et al. 2016; Hattne et al. 2015).

4.5 Detector Specifications

A recent revolution in electron detectors has produced devices capable of rapidly counting electrons. However, a typical electron microscope might be equipped with any number of detectors, ranging from film systems to the newest electron detectors. Rather than cover such a broad spectrum of options, we focus on the important features required of a detector to collect high-quality diffraction micrographs in a MicroED experiment. Because most MicroED data reported to date have been recorded on a CMOS camera manufactured by the TVIPS corporation (TVIPS TemCam model F416) (Hattne et al., 2015), we highlight features present in this system that make MicroED possible. This model contains a square sensor with 4000 pixels on each side, where each square pixel is approximately 15 μm on a side. The total sensor size is thus about 60 mm on a side. For the purposes of noise reduction and memory efficiency, the images are compressed on camera using a 2-by-2 binning operation. The lowest measurable resolution is dictated by beam stop geometry and position in the electron microscope. Ultimately, a sensor size and camera length must be carefully chosen to match the desired resolution range for a given micrograph. CMOS sensors are preferred over slower CCDs for high-speed data collection due to their faster write times and since CMOS detectors do not suffer from blooming artifacts as do CCDs. A scintillator optimized for sensitivity is also beneficial. However, devices and/or settings with less sensitivity and slower read out times can still be used in precession electron diffraction. These considerations change when other types of electron detectors are used. Evaluation of electron diffraction measurements using new devices is ongoing (Nederlof, van Genderen, Li, & Abrahams, 2013). Across the different types of direct electron detectors, dynamic range must be considered to avoid detector damage and maintain accurate counts for all measured reflections.

5. PROCESSING OF MicroED DATA

5.1 Conversion and Processing of Diffraction Images

The types of detectors used in MicroED data collection are not currently suited to save measured data in typical crystallographic formats. While software has been written to specifically process still diffraction images collected

by MicroED (Iadanza & Gonen, 2014), conversion tools have also been developed to port data collected on TVIPS CMOS detectors to the SMV crystallographic data format (Hattne et al., 2015) and are available for download at https://www.janelia.org/sites/default/files/tvips-tools-0.0.0.tgz. The benefit of the latter is that most software toolboxes for crystallographic data processing can recognize the SMV format, making processing of MicroED data as facile and rapid as is processing of data collected at modern X-ray sources. Several factors must be considered when interpreting MicroED data using standard crystallographic analysis pipelines. We review these briefly since many have been detailed elsewhere (Hattne et al., 2015).

First we consider differences in the curvature of the Ewald sphere between X-rays and electron diffraction data. With X-rays, the curvature of the sphere is relevant and often obvious in diffraction images by the appearance of loons (Fig. 1). In contrast, because of the miniscule wavelength of the electrons used for MicroED, at 200 KeV, where the wavelength is approximately 0.025 Å, the curvature of the Ewald sphere is negligible (Fig. 1). For example, at this energy, a 1 Å reflection would experience only a mere fraction of a degree of curvature on the Ewald sphere. By comparison, to achieve similar resolution using monochromatic 12 KeV X-rays that curvature grows to tens of degrees. This difference has practical implications. One is that in diffraction images collected by MicroED information in the direction normal to the sphere is limited. This is a major reason for why indexing from a single-diffraction image is not possible (Hattne et al., 2015; Shi et al., 2013) unless one has a priori knowledge of the unit cell dimensions (Jiang, Georgieva, Zandbergen, & Abrahams, 2009). Indexing without a priori knowledge of the unit cell can be achieved in practice, as has been demonstrated in MicroED with data that covers a phi range of ~30 degree (Nannenga, Shi, Leslie, et al., 2014). A benefit is that particular orientations of a crystal can lead to the Ewald sphere intercepting an entire zone of the reciprocal lattice, simultaneously revealing many Bragg reflections. Another important consequence is the need for accurate knowledge of experimental geometry during data collection, including beam position, camera length, and tilt ranges (Table 1). When partial reflections are measured, this problem is confounded and can lead to further inaccuracies in assignment of intensities to particular reflections.

Second we consider crystal mosaicity, a concept common to macromolecular X-ray crystallography. A model for mosaicity within a macroscopic protein crystal illuminated by a perfectly parallel X-ray beam presents the crystal as an ensemble of lattice blocks with small deviations from the global orientation of the ensemble. The size of these blocks and their relative

deviations from the ensemble orientation can be modeled based on the reflections that appear in a diffraction image (Leslie, 2006; Leslie & Powell, 2007). This model makes simultaneous refinement of mosaicity, experimental geometry, and beam divergence difficult (Leslie, 2006). As crystals shrink to the size of a single mosaic block, the overall lattice should appear ideal. In MicroED, diffracted crystals are only a few hundred nanometers thin, and no larger than a few microns in length and width. Such small crystals should in principle contain fewer mosaic blocks and bear greater influence from the persistence length of the lattice (Dorset, 1980; Nederlof, Li, van Heel, & Abrahams, 2013; Subramanian, Basu, Liu, Zuo, & Spence, 2015). However, if after refinement of experimental parameters errors remain unaccounted for, these may become absorbed by mosaicity and limit its representation of lattice disorder (Hattne et al., 2015).

Lastly, we consider the integration of intensities and its sources of error. As with macromolecular X-ray crystallography, in MicroED, identification of reflections is followed by integration and background correction. The accuracy of integration depends on proper fitting of spot profiles (Kabsch, 2010; Leslie, 1999, 2006) (Fig. 4). Since in MicroED most crystals are small enough to be fully bathed by the electron beam, the shapes of reflections are dictated primarily by the shape transform of the crystal, its unit cell count, and lattice order (Robinson, Vartanyants, Williams, Pfeifer, & Pitney, 2001). The value of background pixels in regions that surround Bragg reflections have also been investigated, with new corrections introduced for truncated values that appear when using equipment not sensitive to low-intensity measurements (Hattne et al., 2015). Several software packages for crystallographic data reduction can accurately estimate reflection profiles during integration (Kabsch, 2010; Leslie & Powell, 2007). Local background near the integrated reflections must also be accounted for. In MicroED this is in principle affected by detector noise, stray light sources in the column, and other sources of incoherent scattering including inelastically scattered electrons. Despite these potential sources of error, MicroED images can show high-quality diffraction even at atomic resolution (Fig. 4).

Multiple-scattering phenomena have been predicted to influence and perhaps overwhelm structure determination by electron diffraction from 3D crystals (Diaz-Avalos et al., 2003; Glaeser & Ceska, 1989; Grigorieff & Henderson, 1996; Spence, 2013; Subramanian et al., 2015). However, recent structures obtained from crystals hundreds of nanometers thick (Table 2) suggest that the theory does not agree with experiment and a more comprehensive theory may be required to account for data obtained by MicroED.

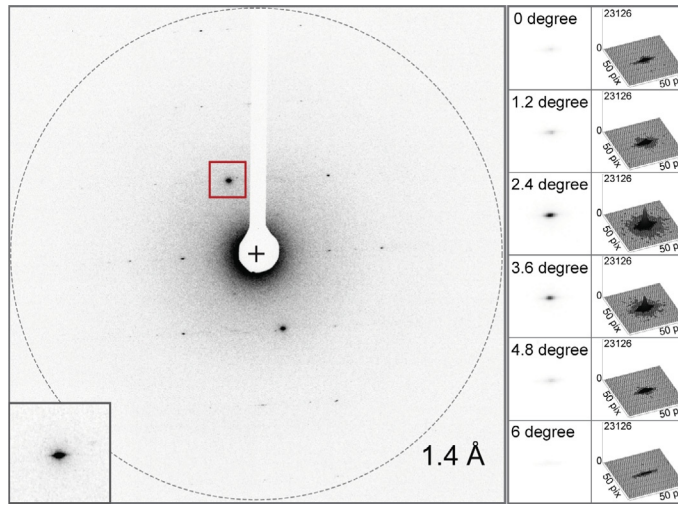

Fig. 4 Properties of high-resolution MicroED patterns. A high-resolution diffraction micrograph (*left*) obtained by MicroED from a crystal of an amyloid peptide (Rodriguez et al., 2015) is shown. An inset and corresponding *red* (*gray* in the print version) *box* highlight a single Bragg reflection that crosses the Ewald sphere at this crystal orientation. The resolution at the edge of the detector is marked. This same reflection is tracked over an angular range of 6 degree (*right*). Profiles of the spot are shown as well as three-dimensional plots of the intensities for the pixels that comprise the spot within a 50-by-50-pixel area. Intensity is shown on the *z*-axis and ranges from 0 to 23126 counts. Each image represents a 1.2 degree wedge through reciprocal space. The start of the wedge is marked on the upper left hand corner of each image; the first of these begins at 0 degree.

Improvements to the theory will require better treatment of crystalline order, eg, lattice bending and disorder, a more comprehensive evaluation of zones, other than major zone axes, an account of rotation or precession during measurement, and a better treatment of experimental sources of noise and error.

5.2 Structure Determination and Refinement

The accurate determination of high-resolution structures in MicroED relies on the same standards for data quality required by X-ray crystallography. Metrics that are optimized to ensure success in structure determination include errors in integration and merging, completeness, and redundancy. The values found in MicroED data for these metrics are generally within the realm encountered in an X-ray crystallography experiment (Hattne et al., 2015; Nannenga, Shi, Hattne, et al., 2014; Nannenga, Shi, Leslie, et al., 2014; Rodriguez et al., 2015; Shi et al., 2013). When crystal

symmetry is low and crystals lie randomly on an EM grid, diffraction data from multiple crystals can be merged to increase completeness. Continuous rotation data collection improves the accuracy of estimates for reflection intensities and therefore reduces the errors observed in data reduction (Nannenga, Shi, Leslie, et al., 2014; Rodriguez et al., 2015).

For MicroED data that meet these criteria, molecular replacement using known structures as probes provides accurate structure solutions, even for previously unknown structures (Rodriguez et al., 2015). Several crystallographic structure determination software packages have been used to solve macromolecular structures from MicroED data; these use electron form factors for structure determination and refinement (Adams et al., 2010; Murshudov et al., 2011). While all structures determined by MicroED have thus far required known atomic models as probes, the accuracy of these solutions is strengthened by the recovery of ligands and side chains during refinement that were omitted from the probe structure (Fig. 3) (Nannenga, Shi, Hattne, et al., 2014; Shi et al., 2013). Errors in the final structures have been comparable to those observed for macromolecular structures determined by X-ray crystallographic methods.

6. SUMMARY AND OUTLOOK

MicroED is a new cryo-EM method. It joins the present revolution in electron microscopy that drives renewed interest in fundamental properties of electrons and their interactions with matter, improved software algorithms for data collection and reduction, and new and more efficient instruments and detectors. These improvements are sure to drive the method beyond its current limits. With further improvements, questions arise: What are the size limits, large and small, for crystals in MicroED? Will very large unit cell dimensions be limiting? How much crystalline disorder can be tolerated? Can dynamics be probed? What general phasing methods are applicable to MicroED? How much damage is inflicted on crystals during MicroED and can structures be obtained with minimal to no visible damage? Can the structure of any well-ordered submicron thick crystal be determined by MicroED? The answer to these questions will herald a new age for the marriage of macromolecular crystallography and cryo-EM.

ACKNOWLEDGMENTS

We thank HHMI for support. J.A.R. was supported by the Giannini Foundation.

REFERENCES

Adams, P. D., Afonine, P. V., Bunkóczi, G., Chen, V. B., Davis, I. W., Echols, N., et al. (2010). PHENIX: A comprehensive Python-based system for macromolecular structure solution. *Acta Crystallographica. Section D, Biological Crystallography*, *66*, 213–221.

Adrian, M., Dubochet, J., Lepault, J., & McDowall, A. W. (1984). Cryo-electron microscopy of viruses. *Nature*, *308*, 32–36.

Batson, P. E., Dellby, N., & Krivanek, O. L. (2002). Sub-ångstrom resolution using aberration corrected electron optics. *Nature*, *418*, 617–620.

Bethe, H. A., Rose, M. E., & Smith, L. P. (1938). The multiple scattering of electrons. *Proceedings of the American Philosophical Society*, *78*, 573–585.

Cheng, Y., Grigorieff, N., Penczek, P. A., & Walz, T. (2015). A primer to single-particle cryo-electron microscopy. *Cell*, *161*, 438–449.

Christensen, A. K. (1971). Frozen thin sections of fresh tissue for electron microscopy, with a description of pancreas and liver. *The Journal of Cell Biology*, *51*, 772–804.

Cowley, C. W. (1964). Cryobiology as viewed by the engineer. *Cryobiology*, *51*, 40–43.

Cowley, J. M. (1969). Image contrast in a transmission scanning electron microscope. *Applied Physics Letters*, *15*, 58–59.

Crowther, R. A., DeRosier, D. J., & Klug, A. (1970). The reconstruction of a three-dimensional structure from projections and its application to electron microscopy. *Proceedings of the Royal Society A: Mathematical, Physical & Engineering Sciences*, *317*, 319–340.

Danev, R., & Nagayama, K. (2001). Transmission electron microscopy with Zernike phase plate. *Ultramicroscopy*, *88*, 243–252.

Davisson, C., & Germer, L. H. (1927a). Diffraction of electrons by a crystal of nickel. *Physics Review*, *30*, 705–740.

Davisson, C., & Germer, L. H. (1927b). The scattering of electrons by a single crystal of nickel. *Nature*, *119*, 558–560.

Deisenhofer, J., Epp, O., Miki, K., Huber, R., & Michel, H. (1985). Structure of the protein subunits in the photosynthetic reaction centre of Rhodopseudomonas viridis at 3 Å resolution. *Nature*, *318*, 618–624.

DeRosier, D. J., & Klug, A. (1968). Reconstruction of three dimensional structures from electron micrographs. *Nature*, *217*, 130–134.

Diaz-Avalos, R., Long, C., Fontano, E., Balbirnie, M., Grothe, R., Eisenberg, D., et al. (2003). Cross-beta order and diversity in nanocrystals of an amyloid-forming peptide. *Journal of Molecular Biology*, *330*, 1165–1175.

Dobro, M. J., Melanson, L. A., Jensen, G. J., & McDowall, A. W. (2010). Chapter three—Plunge freezing for electron cryomicroscopy. In G. J. Jensen (Ed.), *Methods in enzymology* (pp. 63–82): Academic Press.

Dorset, D. L. (1980). Electron diffraction intensities from bent molecular organic crystals. *Acta Crystallographica. Section A*, *36*, 592–600.

Dorset, D. L., & Hauptman, H. A. (1976). Direct phase determination for quasi-kinematical electron diffraction intensity data from organic microcrystals. *Ultramicroscopy*, *1*, 195–201.

Glaeser, R. M. (2008). Cryo-electron microscopy of biological nanostructures. *Physics Today*, *61*, 48–54.

Glaeser, R. M., & Ceska, T. A. (1989). High-voltage electron diffraction from bacteriorhodopsin (purple membrane) is measurably dynamical. *Acta Crystallographica. Section A*, *45*, 620–628.

Gonen, T. (2013). The collection of high-resolution electron diffraction data. In I. Schmidt-Krey & Y. Cheng (Eds.), *Electron crystallography of soluble and membrane proteins* (pp. 153–169): Humana Press.

Gonen, T., Cheng, Y., Sliz, P., Hiroaki, Y., Fujiyoshi, Y., Harrison, S. C., et al. (2005). Lipid–protein interactions in double-layered two-dimensional AQP0 crystals. *Nature*, *438*, 633–638.

Gonen, T., Sliz, P., Kistler, J., Cheng, Y., & Walz, T. (2004). Aquaporin-0 membrane junctions reveal the structure of a closed water pore. *Nature*, *429*, 193–197.

Grassucci, R. A., Taylor, D. J., & Frank, J. (2007). Preparation of macromolecular complexes for cryo-electron microscopy. *Nature Protocols*, *2*, 3239–3246.

Grigorieff, N., & Henderson, R. (1996). Comparison of calculated and observed dynamical diffraction from purple membrane: Implications. *Ultramicroscopy*, *65*, 101–107.

Grubb, D. T. (1971). The calibration of beam measurement devices in various electron microscopes, using an efficient Faraday cup. *Journal of Physics E*, *4*, 222.

Haider, M., Rose, H., Uhlemann, S., Schwan, E., Kabius, B., & Urban, K. (1998). A spherical-aberration-corrected 200 kV transmission electron microscope. *Ultramicroscopy*, *75*, 53–60.

Hattne, J., Reyes, F. E., Nannenga, B. L., Shi, D., de la Cruz, M. J., Leslie, A. G. W., et al. (2015). MicroED data collection and processing. *Acta Crystallographica. Section A, Foundations and Advances*, *71*, 353–360.

Hattne, J., Shi, D., de la Cruz, J., Reyes, F. E., & Gonen, T. (2016). Modeling truncated intensities of faint reflections in MicroED images. *Journal of Applied Crystallography*, *49*. http://dx.doi.org/10.1107/S1600576716007196.

Haupert, L. M., & Simpson, G. J. (2011). Screening of protein crystallization trials by second order nonlinear optical imaging of chiral crystals (SONICC). *Methods (San Diego Calif.)*, *55*, 379–386.

Held, G. (2012). Low-energy electron diffraction: Crystallography of surfaces and interfaces. In R. Schäfer & P. C. Schmidt (Eds.), *Methods in physical chemistry* (pp. 625–642). Weinheim: Wiley-VCH Verlag GmbH & Co. KGaA.

Henderson, R. (1995). The potential and limitations of neutrons, electrons and X-rays for atomic resolution microscopy of unstained biological molecules. *Quarterly Reviews of Biophysics*, *28*, 171–193.

Henderson, R., Baldwin, J. M., Ceska, T. A., Zemlin, F., Beckmann, E., & Downing, K. H. (1990). Model for the structure of bacteriorhodopsin based on high-resolution electron cryo-microscopy. *Journal of Molecular Biology*, *213*, 899–929.

Henderson, R., & Unwin, P. N. T. (1975). Three-dimensional model of purple membrane obtained by electron microscopy. *Nature*, *257*, 28–32.

Henkelman, R. M., & Ottensmeyer, F. P. (1974). An energy filter for biological electron microscopy. *Journal of Microscopy*, *102*, 79–94.

Hiroaki, Y., Tani, K., Kamegawa, A., Gyobu, N., Nishikawa, K., Suzuki, H., et al. (2006). Implications of the aquaporin-4 structure on array formation and cell adhesion. *Journal of Molecular Biology*, *355*, 628–639.

Iadanza, M. G., & Gonen, T. (2014). A suite of software for processing MicroED data of extremely small protein crystals. *Journal of Applied Crystallography*, *47*, 1140–1145.

Iancu, C. V., Tivol, W. F., Schooler, J. B., Dias, D. P., Henderson, G. P., Murphy, G. E., et al. (2007). Electron cryotomography sample preparation using the Vitrobot. *Nature Protocols*, *1*, 2813–2819.

Jap, B. K., Downing, K. H., & Walian, P. J. (1990). Structure of PhoE porin in projection at 3.5 Å resolution. *Journal of Structural Biology*, *103*, 57–63.

Jiang, L., Georgieva, D., Zandbergen, H. W., & Abrahams, J. P. (2009). Unit-cell determination from randomly oriented electron-diffraction patterns. *Acta Crystallographica. Section D, Biological Crystallography*, *65*, 625–632.

Kabsch, W. (2010). XDS. *Acta Crystallographica. Section D, Biological Crystallography*, *66*, 125–132.

Koster, A. J., Chen, H., Sedat, J. W., & Agard, D. A. (1992). Automated microscopy for electron tomography. *Ultramicroscopy*, *46*, 207–227.

Kühlbrandt, W., Wang, D. N., & Fujiyoshi, Y. (1994). Atomic model of plant light-harvesting complex by electron crystallography. *Nature*, *367*, 614–621.

Lepper, S., Merkel, M., Sartori, A., Cyrklaff, M., & Frischknecht, F. (2010). Rapid quantification of the effects of blotting for correlation of light and cryo-light microscopy images. *Journal of Microscopy*, *238*, 21–26.

Leslie, A. G. W. (1999). Integration of macromolecular diffraction data. *Acta Crystallographica. Section D, Biological Crystallography*, *55*, 1696–1702.

Leslie, A. G. W. (2006). The integration of macromolecular diffraction data. *Acta Crystallographica. Section D, Biological Crystallography*, *62*, 48–57.

Leslie, A. G. W., & Powell, H. R. (2007). Processing diffraction data with mosflm. In R. J. Read & J. L. Sussman (Eds.), *Evolving methods for macromolecular crystallography* (pp. 41–51). The Netherlands: Springer.

Morishita, S., Yamasaki, J., & Tanaka, N. (2013). Measurement of spatial coherence of electron beams by using a small selected-area aperture. *Ultramicroscopy*, *129*, 10–17.

Murshudov, G. N., Skubák, P., Lebedev, A. A., Pannu, N. S., Steiner, R. A., Nicholls, R. A., et al. (2011). *REFMAC* 5 for the refinement of macromolecular crystal structures. *Acta Crystallographica. Section D, Biological Crystallography*, *67*, 355–367.

Nannenga, B. L., & Gonen, T. (2014). Protein structure determination by MicroED. *Current Opinion in Structural Biology*, *27*, 24–31.

Nannenga, B. L., Shi, D., Hattne, J., Reyes, F. E., & Gonen, T. (2014b). Structure of catalase determined by MicroED. *eLife*, *3*, e03600.

Nannenga, B. L., Shi, D., Leslie, A. G. W., & Gonen, T. (2014a). High-resolution structure determination by continuous-rotation data collection in MicroED. *Nature Methods*, *11*, 927–930.

Nederlof, I., Li, Y. W., van Heel, M., & Abrahams, J. P. (2013). Imaging protein three-dimensional nanocrystals with cryo-EM. *Acta Crystallographica. Section D, Biological Crystallography*, *69*, 852–859.

Nederlof, I., van Genderen, E., Li, Y.-W., & Abrahams, J. P. (2013). A Medipix quantum area detector allows rotation electron diffraction data collection from submicrometre three-dimensional protein crystals. *Acta Crystallographica. Section D, Biological Crystallography*, *69*, 1223–1230.

Oleynikov, P., Hovmöller, S., & Zou, X. D. (2007). Precession electron diffraction: Observed and calculated intensities. *Ultramicroscopy*, *107*, 523–533.

Robinson, A. L. (1986). Electron microscope inventors share Nobel physics prize: Ernst Ruska built the first electron microscope in 1931; Gerd Binnig and Heinrich Rohrer developed the scanning tunneling microscope 50 years later. *Science*, *234*, 821–822.

Robinson, I. K., Vartanyants, I. A., Williams, G. J., Pfeifer, M. A., & Pitney, J. A. (2001). Reconstruction of the shapes of gold nanocrystals using coherent X-Ray diffraction. *Physical Review Letters*, *87*, 195505.

Rodriguez, J. A., Ivanova, M. I., Sawaya, M. R., Cascio, D., Reyes, F. E., Shi, D., et al. (2015). Structure of the toxic core of α-synuclein from invisible crystals. *Nature*, *525*, 486–490.

Ruskin, R. S., Yu, Z., & Grigorieff, N. (2013). Quantitative characterization of electron detectors for transmission electron microscopy. *Journal of Structural Biology*, *184*, 385–393.

Shi, D., Nannenga, B. L., de la Cruz, J. M., Liu, J., Sawtelle, S., Calero, G., et al. (2016). The collection of MicroED data for macromolecular crystallography. *Nature Protocols*, *11*, 895–904.

Shi, D., Nannenga, B. L., Iadanza, M. G., & Gonen, T. (2013). Three-dimensional electron crystallography of protein microcrystals. *eLife*, *2*, e01345.

Spence, J. C. H. (2013). *High-resolution electron microscopy*. Oxford: OUP.

Stern, R. M., & Taub, H. (1970). An introduction to the dynamical scattering of electrons by crystals. *C R C Critical Reviews in Solid State Sciences*, *1*, 221–302.

Subramanian, G., Basu, S., Liu, H., Zuo, J.-M., & Spence, J. C. H. (2015). Solving protein nanocrystals by cryo-EM diffraction: Multiple scattering artifacts. *Ultramicroscopy*, *148*, 87–93.

Taylor, K. A., & Glaeser, R. M. (1976). Electron microscopy of frozen hydrated biological specimens. *Journal of Ultrastructure Research*, *55*, 448–456.
Thomas, L. E. (1970). The diffraction-dependence of electron damage in a high voltage electron microscope. *Radiation Effects*, *5*, 183–194.
Thomson, G. P., & Reid, A. (1927). Diffraction of cathode rays by a thin film. *Nature*, *119*, 890.
Walz, T., & Grigorieff, N. (1998). Electron crystallography of two-dimensional crystals of membrane proteins. *Journal of Structural Biology*, *121*, 142–161.
Walz, T., Hirai, T., Murata, K., Heymann, J. B., Mitsuoka, K., Fujiyoshi, Y., et al. (1997). The three-dimensional structure of aquaporin-1. *Nature*, *387*, 624–627.
Weathersby, S. P., Brown, G., Centurion, M., Chase, T. F., Coffee, R., Corbett, J., et al. (2015). Mega-electron-volt ultrafast electron diffraction at SLAC National Accelerator Laboratory. *The Review of Scientific Instruments*, *86*, 073702.
Yonekura, K., Kato, K., Ogasawara, M., Tomita, M., & Toyoshima, C. (2015). Electron crystallography of ultrathin 3D protein crystals: Atomic model with charges. *Proceedings of the National Academy of Sciences*, *112*, 3368–3373.
Zanchi, G., Sevely, J., & Jouffrey, B. (1977). An energy filter for high voltage electron microscopy. *Journal of Electron Spectroscopy and Related Phenomena*, *2*, 95–104.
Zuo, J. M., Gao, M., Tao, J., Li, B. Q., Twesten, R., & Petrov, I. (2004). Coherent nano-area electron diffraction. *Microscopy Research and Technique*, *64*, 347–355.